GEOPHYSICS, VOL. 64, NO. 3 (MAY-JUNE 1999); P. 942–953, 17 FIGS.

Factors affecting spatial resolution

Gijs J. O. Vermeer*

ABSTRACT

The theory of spatial resolution has been well-established in various papers dealing with inversion and prestack migration. Nevertheless, there is a continuing flow of papers being published on spatial resolution, in particular in relation to spatial sampling. This paper continues the discussion, and deals with various factors affecting spatial resolution.

The theoretical best-possible resolution can be predicted using Beylkin's formula. This formula gives answers on the effect on resolution of frequency, aperture, offset, and acquisition geometry. In this paper, these factors are investigated using a single diffractor in a constant-velocity medium. Some simple resolution formulas are derived for 2-D zero-offset data. These formulas are similar to formulas derived elsewhere in a more heuristic way, and which are in common use in the industry. The formulas are extended to 2-D common-offset data.

The width of the spatial wavelet resulting from migration of the diffraction event is compared with the resolution predicted from Beylkin's formula for various 3-D single-fold data sets. The measured widths confirm the theoretical prediction that zero-offset data produce the best possible resolution and 3-D shots the worst, with common-offset gathers and cross-spreads scoring intermediate.

The effects of sampling and fold cannot be derived directly from Beylkin's formula; these effects are analyzed by looking at the migration noise rather than at the width of the spatial wavelet. Random coarse sampling may produce somewhat less migration noise than regular coarse sampling, though it cannot be as good as regular dense sampling. The bin-fractionation technique (which achieves finer midpoint sampling without changing the station spacings) does not achieve higher resolution than conventional sampling.

Generally speaking, increasing fold does not improve the theoretically best possible resolution. However, as noise always has a detrimental effect on the resolvability of events, fold—by reducing noise—will improve resolution in practice. This also applies to migration noise as a product of coarse sampling.

INTRODUCTION

The theory of spatial resolution has been dealt with in great detail by various authors on prestack migration and inversion (e.g., Berkhout, 1984; Beylkin, 1985; Beylkin et al., 1985; Cohen et al., 1986; Bleistein, 1987) and on diffraction tomography (e.g., Wu and Toksöz, 1987). Despite all this work, the practical consequences of the theory are still open to much debate.

Von Seggern (1994) discusses resolution for various 3-D geometries, and concludes: "Uniform 3-D patterns, asymmetric patterns, and both narrow and wide swath 3-D patterns all produce nearly equivalent images of a point scatterer, without significantly better resolution in one or the other horizontal direction." These results were obtained using quite a coarse measurement technique; moreover, fold varied across the midpoint range. As a consequence, the considerable differences in resolution that do occur between different geometries were overlooked.

Neidell (1994) submitted that coarse sampling, if compensated by high fold (24-fold or higher), does not sacrifice resolution. His conjecture led to a flurry of reactions (Ebrom et al., 1995b; Neidell, 1995; Vermeer, 1995; Markley et al., 1996).

Ebrom et al. (1995b) and Markley et al. (1996) investigate resolution using a tank model consisting of a number of vertical rods. The time slices at the level of the top of the rods are compared for various sampling intervals and folds of coverage. Whereas Ebrom et al. (1995b) showed that the resolution in the time slice could be finer than the acquisition common midpoint (CMP) binning, Markley et al. (1996) conclude that finer CMP binning improves the image significantly compared to coarse binning with the same number of traces, thus contradicting Neidell's (1994) conjecture.

Published on Geophysics Online February 12, 1999. Manuscript received by the Editor June 25, 1997; revised manuscript received September 21, 1998.
*3DSymSam, Maduroweg 3, 2252 TS Voorschoten, The Netherlands. E-mail: vermeerg@worldonline.nl.

The issue of sampling is expanded further with the introduction of quasi-random sampling (Zhou and Schuster, 1995; Sun et al., 1997). Zhou and Schuster (1995) demonstrate that quasi-random coarse sampling may lead to less migration artifacts than regular coarse sampling. Sun et al. (1997) conclude that migration of data sampled with the quasi–Monte Carlo technique can reduce the computational work load by a factor of 4 or more. These results might be interpreted as "random sampling is superior to regular acquisition for purposes of noise reduction" (Bednar, 1996), a statement that assumes that the (coherent) noise is coarsely sampled. Sun et al.'s (1997) conclusion is questioned in Vermeer (1998b).

Apart from the authors mentioned in the first paragraph, none of the above authors mentioned Beylkin's formula for spatial resolution, even though it had already been published in 1985 (Beylkin, 1985). The present paper uses Beylkin's formula to derive resolution formulas for simple cases and to explain results obtained for various configurations. Lavely et al. (1997) and Gibson et al. (1998) also use Beylkin's formula as a starting point for resolution analysis.

Levin (1998) provides a lucid narrative of the resolution of dipping reflectors. The present paper, although not dealing explicitly with reflectors, confirms many insights offered in that paper, which is recommended for further reading.

In conventional seismic acquisition, the measurements are carried out at or close to the surface, basically in one horizontal plane. This measurement configuration leads to quite a difference between the resolution in the vertical direction and the resolution in a plane parallel to the measurement plane. This paper deals only with such configurations; hence, it does not discuss the resolution of measurements at various depth levels, such as made with vertical seismic profiling (VSPs).

Resolution is about the resolvability of two close events. This resolvability is determined by the width of the main lobe of the wavelet and by the strength of the side lobes relative to the main lobe. In this paper, I leave the effect of side lobes mostly aside; I concentrate on measurements of the width of the wavelet after migration. [For a detailed discussion of the effect of sidelobes, see Berkhout (1984). In particular if two events have different strengths, side lobes of the strong event may mask the main peak of the weak event.] The wider the wavelet, the larger the distance between two events needs to be for their resolvability. The smallest distance for which two events can still be distinguished is called the minimum resolvable distance.

The theory of resolution leads to a potential resolution (i.e., the best possible resolution for a given source wavelet), velocity model, shot/receiver configuration, and some position of the output point. The potential resolution can only be achieved if the wavefield is properly sampled. Next to potential resolution, this paper also uses achievable resolution, which is defined as the best possible resolution that can be achieved in practice. Events which do not satisfy the velocity model, migration noise caused by coarse sampling, and other types of noise all affect resolvability; hence, the achievable resolution is not as good as the potential resolution.

How to measure temporal resolution has been the subject of various papers. In a classic paper, Kallweit and Wood (1982) discuss how various criteria (Rayleigh, Ricker, Widess criteria) can be used to describe the width of a wavelet as a measure of temporal resolution. They conclude that (potential) resolution is proportional to maximum frequency (strictly speaking, to frequency bandwidth; Knapp, 1990). In this paper, their results are extended into the realm of spatial resolution, i.e., spatial resolution is proportional to maximum wavenumber, and the minimum resolvable distance is inversely proportional to maximum wavenumber.

This paper is structured as follows. The paper starts with a summary of the main points on spatial resolution as made in Beylkin et al. (1985) and applies this theory to a constant-velocity medium. This leads naturally to similar resolution formulas (for 2-D data) as given in Ebrom et al. (1995a) with an extension to offset data. In the next part, I illustrate various aspects of spatial resolution (aperture, offset, acquisition geometry) using a single diffractor in a constant-velocity medium (the same model as used in von Seggern, 1994). The width of the spatial wavelet after migration is used as a measure in the resolution comparisons. Finally, I discuss why sampling is important, even though the sampling interval does not appear in the resolution formulas, and I discuss the influence of fold. A poster version of this paper was published as Vermeer (1998a).

SPATIAL RESOLUTION FORMULAS

Spatial resolution—the link with migration/inversion

In the literature, true-amplitude prestack migration formulas have been derived for single-fold 3-D data sets with two spatial coordinates ξ_1 and ξ_2, and traveltime t or frequency f as the third coordinate. The coordinates ξ_1 and ξ_2 describe the shot/receiver configuration. That is, for fixed X and fixed Y, $\mathbf{x_s} = (X, Y, 0)$ and $\mathbf{x_r} = (\xi_1, \xi_2, 0)$ describe a 3-D common-shot gather, and $\mathbf{x_s} = (\xi_1, Y, 0)$ and $\mathbf{x_r} = (X, \xi_2, 0)$ describe a cross-spread. Note that these data sets are the same data sets introduced as subsets of various 3-D geometries in Vermeer (1994, 1998c), and which are called minimal data sets in Padhi and Holley (1997).

Beylkin (1985) and Beylkin et al. (1985) derive formulas to compute ("reconstruct") acoustic impedance contrast as a function of position $\mathbf{x}(x, y, z)$ from seismic measurements with limited aperture. The limited aperture is defined by the range of $\xi = (\xi_1, \xi_2)$. They show that in this process, the observed data are transformed into reconstructed data using a mapping of (ξ_1, ξ_2, f) (the coordinates of the observed data) to (k_x, k_y, k_z) (the coordinates of the reconstructed data). The mapping is given by

$$\mathbf{k} = f \nabla_x \phi(\mathbf{x}, \boldsymbol{\xi}), \tag{1}$$

in which $\mathbf{k} = (k_x, k_y, k_z)$ is the wavenumber vector in the reconstructed (migration) domain, and $\phi(\mathbf{x}, \boldsymbol{\xi})$ is the traveltime surface (also called migration operator) of a diffractor in $\mathbf{x}$ for shot/receiver pairs described by $\boldsymbol{\xi}$. $\nabla_x \phi(\mathbf{x}, \boldsymbol{\xi})$ represents the derivative of $\phi(\mathbf{x}, \boldsymbol{\xi})$ with respect to the point of reconstruction (output point) $\mathbf{x}$; $\phi(\mathbf{x}, \boldsymbol{\xi})$ has to be computed from the background model (velocity model).

Equation (1) maps the 5-D traveltime surface $\phi(\mathbf{x}, \boldsymbol{\xi})$ to 3-D wavenumber. This mapping corresponds to the fact that in prestack migration, each input trace described by ξ is used in the reconstruction of a volume of output points (x, y, z). Equation (1) determines the region of coverage D_x in the spatial wavenumber domain (the 3-D spatial bandwidth). Beylkin et al. (1985) state, "the description of D_x is, in fact, the estimate

of spatial resolution." The larger the region of coverage in **k**, the better the potential resolution.

To further explain the meaning of equation (1), it is worthwhile quoting Beylkin et al. (1985) (with minor modifications to reflect the notation used in this paper):

> The mapping equation (1) is of fundamental importance with respect to inversion algorithms. It shows how the total domain of integration (ξ_1, ξ_2, f) on which our data are defined is related to region of coverage in the domain of spatial frequencies.
>
> To summarize, the spatial resolution at a given point **x** defined by the region D_x depends on
> i) the total domain of integration, which is determined by the configuration of sources and receivers and the frequency band of the signal, and
> ii) the mapping equation (1) of this domain into the domain of spatial frequencies, which is determined by the background model and can be obtained numerically by raytracing. This mapping is different for each point of reconstruction.
>
> Together i) and ii) determine the limits on spatial resolution at each point of reconstruction given the configuration of experiment and the background model.

Beylkin's formula [equation (1)] makes analysis of potential resolution quite simple: It should be possible to explain many resolution tests by analyzing the spatial gradients of the diffraction traveltime surfaces $\phi(\mathbf{x}, \boldsymbol{\xi})$ in the given experiment configuration.

It is not (always) necessary to analyze the full coverage in **k**. As follows from Kallweit and Wood (1982), the maximum wavenumber [corresponding to maximum gradients of $\phi(\mathbf{x}, \boldsymbol{\xi})$] can give a fair indication of resolution, provided $\mathbf{k} = 0$ is part of the wavenumber range.

The diffraction traveltime $\phi(\mathbf{x}, \boldsymbol{\xi})$ can be described as

$$\phi(\mathbf{x}, \boldsymbol{\xi}) = \tau(\mathbf{x}, \mathbf{x_s}) + \tau(\mathbf{x}, \mathbf{x_r}) = \tau_s + \tau_r, \tag{2}$$

where $\tau(\mathbf{x}, \mathbf{y})$ is the traveltime from surface position **y** to subsurface position **x**. Similarly, **k** can be written as the vectorial sum

$$\mathbf{k} = \mathbf{k_s} + \mathbf{k_r}, \tag{3}$$

where $\mathbf{k_s}$ and $\mathbf{k_r}$ are the contributions of shot and receiver, respectively, to the wavenumber vector **k**. It can be shown that the directional derivatives of the traveltimes τ_s and τ_r with respect to **x** are in fact the directions of the corresponding raypaths in **x**. Hence, $\mathbf{k_s}$ and $\mathbf{k_r}$ point in the direction of the raypaths at **x** (see Figure 1). Each shot/receiver pair in the geometry corresponds to a point **k** in wavenumber space. Taking all shot/receiver pairs of a configuration leads to a collection of points in wavenumber space.

This mapping of a geometry configuration to wavenumber space is also the subject of many papers dealing in particular with VSP and crosswell resolution analysis (Devaney, 1984; Wu and Toksöz, 1987; Goulty, 1997; Lavely et al., 1997). Goulty (1997) provides a very readable description of this approach. Beylkin's formula describes this mapping in a concise way.

It may be seen immediately from equation (3) and Figure 1 that zero-offset data can potentially produce the highest resolution because $\mathbf{k_s}$ and $\mathbf{k_r}$ coincide in that case.

Before taking the next step, I want to mention that sampling considerations do not appear at all in above discussion. Beylkin et al. (1985) assume, in fact, continuous variables ξ_1 and ξ_2. In other words, because in practice sampling is inevitable, sampling should be dense enough to allow accurate evaluation of the integrals involved in migration. The resolution that can be obtained in that case is the potential resolution, as introduced earlier.

Spatial resolution formulas for constant velocity

It is illuminating to investigate D_x for a medium with constant velocity v and zero-offset geometry. For a point $\mathbf{x}_s = \mathbf{x}_r = (\xi_1, \xi_2, 0)$, substituting of equation (2) into equation (1) leads to

$$\mathbf{k} = 2\left(\frac{x-\xi_1}{d}, \frac{y-\xi_2}{d}, \frac{z}{d}\right) f/v, \tag{4}$$

where d is the distance from the coinciding shot and receiver to the subsurface point **x**. The vector in the parentheses is the unit vector pointing from $\mathbf{x}_s$ to **x**. The left side of Figure 8 depicts equation (4) graphically.

Consider now a 2-D zero-offset geometry laid out along the x-axis. Then the maximum values for k_x and k_z can be written as

$$\begin{aligned} k_{x,\max} &= 2f_{\max} \sin\theta_{x,\max}/v, \\ k_{z,\max} &= 2f_{\max}/v, \end{aligned} \tag{5}$$

where $\theta_{x,\max}$ is the angle between the vertical and the raypath from the output point to the farthest shot/receiver pair.

Note the difference between horizontal and vertical resolution: k_x reaches its maximum for the maximum value of d in the x-direction, whereas k_z reaches its maximum for the minimum value of d (i.e., if $d = z$, then $k_z = 2f/v$). A corollary of these

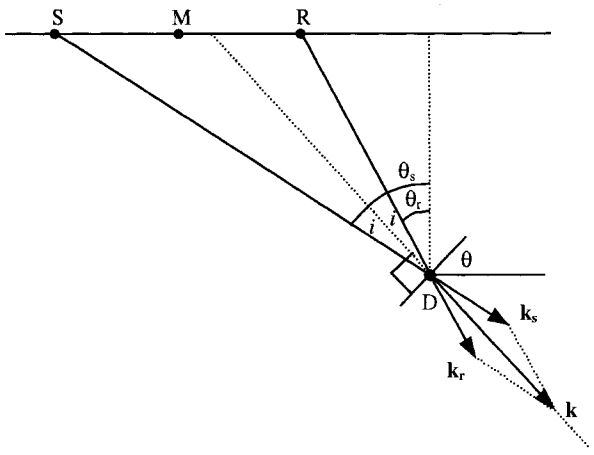

FIG. 1. Illumination of diffractor D by shot/receiver pair S/R. The directions of the raypaths at D determine the shot and receiver wavenumber components of total wavenumber **k**. SD and RD are also the reflection raypaths for a reflector through D with dip angle $\theta = (\theta_s + \theta_r)/2$. The raypaths make an angle $i = (\theta_s - \theta_r)/2$ with **k**.

observations is that horizontal resolution can be improved by using a larger migration aperture (migration radius), thus including a steeper part of the diffraction traveltime curves, whereas vertical resolution does not depend on aperture.

Kallweit and Wood (1982) show that a practical limit for temporal resolution, i.e., the minimum resolvable time interval R_t, is given by the tuning thickness of a zero-phase wavelet, which is the distance between peak and first trough (Rayleigh criterion). For a Ricker wavelet, they show that

$$R_t = \frac{1}{2.6 f_p}, \tag{6a}$$

where f_p is the peak frequency of the Ricker wavelet. For a sinc wavelet, Kallweit and Wood (1982) show that

$$R_t = \frac{1}{1.4 f_{\max}} = \frac{c}{f_{\max}}, \tag{6b}$$

where $f_{\max}$ is the maximum frequency, and the proportionality factor c is 0.71.

Analogously, for spatial frequencies, the minimum resolvable distance in a particular direction α follows from $R_\alpha = c/k_{\alpha,\max}$. Using equation (5), this yields

$$R_x = \frac{cv}{2 f_{\max} \sin\theta_{x,\max}}, \tag{7a}$$

and

$$R_z = \frac{c}{2 f_{\max}}. \tag{7b}$$

With $c = 1/2$, we find the same formulas for horizontal and vertical resolution as given in Ebrom et al. (1995a). For measurements based solely on peak-to-peak or peak-to-trough distances, $c = 1/2$ is too optimistic. However, "below the tuning thickness limit, amplitude information encodes thickness variations provided the entire amplitude variation is caused by tuning effects, and amplitude calibration then permits . . . thickness calculations for arbitrarily thin beds" (Kallweit and Wood, 1982).

[A different, but questionable formula for resolution, is presented in Safar (1985) and quoted in Neidell (1995). Using the same notation as above, equation (7) in Safar (1985) reads

$$R_x = \frac{1.4v}{4 f_{\max} \tan\theta_{x,\max}}, \tag{8}$$

which means that unlimited resolution would be achievable with unlimited aperture.]

Using similar reasoning as for the 2-D zero-offset gather above, it follows that for a 2-D common-offset gather (acquired along the x-axis), the minimum horizontally resolvable distance becomes

$$R_x = \frac{cv}{f_{\max}(\sin\theta_{s,\max} + \sin\theta_{r,\max})}, \tag{9}$$

where $\theta_{s,\max}$ and $\theta_{r,\max}$ are the angles of the vertical with the raypaths as indicated in Figure 1 for the shot/receiver pair with the largest distance of its midpoint M to the output point. Note that equation (9) also applies to a 2-D common-offset gather acquired along a line parallel to the x-axis. In that case, the angles are measured in the plane through acquisition line and output point.

Equation (9) can also be written as (see Figure 1)

$$R_x = \frac{cv}{2 f_{\max} \sin\theta_{x,\max} \cos i}, \tag{10}$$

where $\theta_{x,\max} = (\theta_{s,\max} + \theta_{r,\max})/2$ (i.e., the maximum dip angle illuminated by the shot/receiver pairs), and $i = (\theta_{s,\max} - \theta_{r,\max})/2$ (the angle of incidence of the raypaths for the maximum dip angle).

Note the similarity between equations (7a) and (10): for $i = 0$, equation (10) reduces to equation (7a). Both equations show that the maximum horizontal resolution is closely coupled to the maximum dip angle that can be illuminated.

The vertical resolution that can be reached with a common-offset/common-azimuth gather can be written as

$$R_z = \frac{cv}{2 f_{\max} \cos i}, \tag{11}$$

where i is now the angle for the shot/receiver pair with $\theta_s = -\theta_r$ (i.e., with its midpoint located vertically above the output point). Cos i in equations (10) and (11) describes the NMO stretch effect, which reduces $f_{\max}$ to $f_{\max} \cos i$. As a consequence, for a given midpoint range, the minimum resolvable distance achievable by offset data is larger than for zero-offset data (i.e., resolution is best for zero-offset data).

Before discussing spatial resolution measurements, I would like to make a link with discussions on migration stretch (Tygel et al., 1994; Levin, 1998). Figure 1 illustrates that each shot/receiver pair corresponds to a wavenumber vector $\mathbf{k}$, which is normal to the plane illuminated by the shot/receiver pair. For a plane dipping in the x-direction with angle θ, $\mathbf{k} = (k_x, k_y, k_z) = 2f/v\ (\sin\theta \cos i, 0, \cos\theta \cos i)$, where i is the angle of incidence. The factor $1/\cos\theta \cos i$ is sometimes called the migration stretch factor or vertical pulse distortion (Tygel et al., 1994). Similarly, the factor $1/\sin\theta \cos i$ might be called the horizontal pulse distortion. The larger θ, the larger k_x; hence, the better the horizontal resolution. $\theta_{x,\max}$ is determined by the range of input data or, what is about the same, the migration radius. As argued in Levin (1998), the pulse distortion as a function of θ is only an apparent distortion because the magnitude of $\mathbf{k}$ in the θ direction is not affected by it. Only the cos i factor (NMO stretch factor) affects all components of $\mathbf{k}$ and means a reduction in resolution in all directions. An extensive discussion of these insights is given in Levin (1998).

SPATIAL RESOLUTION MEASUREMENTS

Procedure for resolution analysis

Next, I illustrate various issues relating to resolution based on a model consisting of a single diffractor in (0, 0, 500) in a constant-velocity medium with velocity = 2500 m/s. The source wavelet is a Ricker wavelet with peak frequency $f_p = 50$ Hz. The same model and isotropic source wavelet was used in von Seggern (1994). The starting point is a modified version of von Seggern's equation (1), which was derived from equation (21) of Cohen et al. (1986):

$$f(\mathbf{x}) = \iint d\xi_1\, d\xi_2 h(\mathbf{x}, \boldsymbol{\xi}) p[\phi(\mathbf{x}, \boldsymbol{\xi}) - \phi(0, \boldsymbol{\xi})], \tag{12}$$

where $f(\mathbf{x})$ is image in $\mathbf{x}$, $p[t]$ is source wavelet, and $h(\mathbf{x}, \boldsymbol{\xi})$ is Jacobian of coordinate transformation corresponding to equation (1). $\phi(0, \boldsymbol{\xi})$ is the traveltime surface [equation (2)] of the

actual diffractor, the data, whereas $\phi(\mathbf{x}, \boldsymbol{\xi})$ is the traveltime surface of a diffractor in the output point, i.e., the integration path. $p[\phi(\mathbf{x}, \boldsymbol{\xi}) - \phi(0, \boldsymbol{\xi})]$ picks the value of the wavefield at the correct point in the source wavelet. Amplitude factors normally occurring in the migration formulas cancel in this case as the output point is close to the actual diffractor (von Seggern, 1994).

In von Seggern (1991), it was shown that, for a scatterer, migration of surface data recorded with a Ricker wavelet as a source pulse produces a Gaussian spatial wavelet in the horizontal directions, but maintains the Ricker wavelet in the vertical direction. Figure 2 displays the source wavelet and the corresponding Gaussian wavelet on the same scale. The Gaussian represents the ideal horizontal wavelet.

In the following, I concentrate on measurements of the width of the spatial wavelet in the horizontal direction, this width being representative of the minimum resolvable distance in that direction.

2-D resolution in the zero-offset model

For a varying line length and constant sampling interval of 25 m, and using coinciding shots and receivers along the x-axis, Figure 3 displays the amplitude of a horizontal trace at the depth of the diffractor (500 m). The maximum amplitude of all traces has been normalized to 1. The ideal spatial wavelet is also displayed. It virtually coincides with the wavelet found for a line length of 6000 m. Figure 3 shows that limiting the line length (migration aperture width) leads to wider spatial wavelets. This wavelet stretch is an expression of the horizontal pulse distortion introduced earlier.

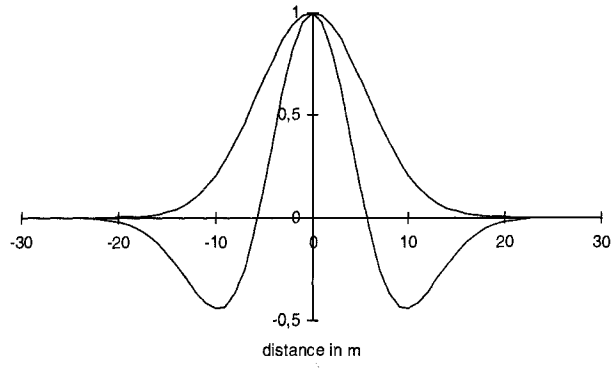

FIG. 2. The basic spatial wavelets used in this paper. The Ricker wavelet and the Gaussian wavelet have been drawn for a peak frequency of 50 Hz and a velocity of 2500 m/s. The Gaussian wavelet is the narrowest achievable bell in prestack migration for the horizontal coordinates.

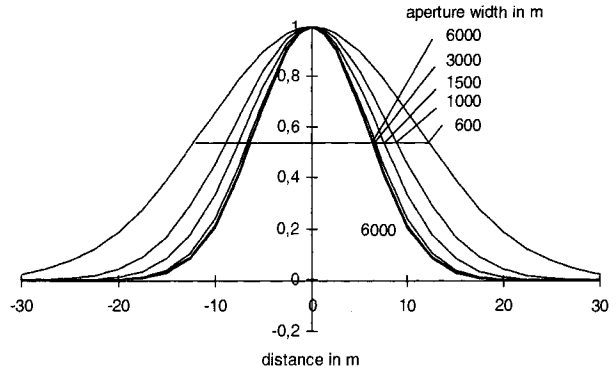

FIG. 3. Horizontal resolution in a 2-D zero-offset geometry for various apertures and a diffractor in (0, 0, 500). Starting with the widest, the wavelets correspond successively to aperture widths 600, 1000, 1500, 3000, and 6000 m. The horizontal line in the center of the figure indicates the level at which widths have been measured for Figures 4 and 5 (width of ideal wavelet is 12.5 m).

I now introduce a measure of width of the various wavelets by defining the width of the ideal wavelet as 12.5 m (horizontal line in Figure 3). Figure 4 tests the hypothesis that this width is representative of maximum wavenumber and of spatial resolution. The squares indicate the measured widths of the wavelets shown in Figure 3, whereas the drawn line represents predicted widths according to

$$w = \frac{v}{4 f_p \sin \theta_{x,\max}}. \tag{13}$$

The choice of proportionality factor 1/4 ensures $w = 12.5$ m for $\sin \theta_{x,\max} = 1$. According to equation (7a), the right-hand side of equation (13) is proportional to minimum resolvable distance ($f_{\max}$ is proportional to f_p). The near-perfect agreement between measured width and predicted width confirms the hypothesis.

2-D resolution in offset model

In Figure 5, the results of different offset experiments have been brought together. As in Figure 4, the widths of the spatial wavelets are measured at the same normalized value (squares), and also computed on basis of a modification of equation (9) (solid curves):

$$w = \frac{v}{2 f_p (\sin \theta_s + \sin \theta_r)}, \tag{14}$$

Each curve represents the results for a single midpoint range. In this case, the agreement between predicted value and measured value is not as good as for the zero-offset data in Figure 4. However, the main trends are caught reasonably well, with increasing discrepancies for increasing line lengths.

For line length 2500 m, the width of the spatial wavelet tends to decrease with increasing offset. For even wider apertures, the width can become smaller than the ideal width (12.5 m) corresponding to the input wavelet. I suspect that this is caused

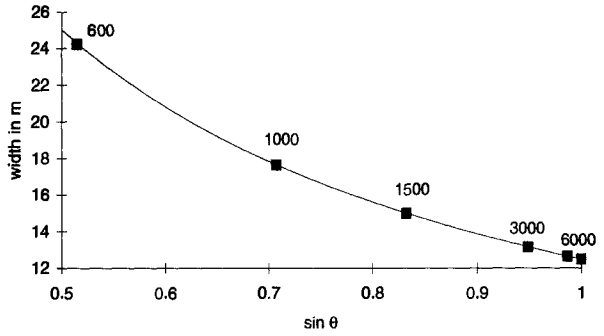

FIG. 4. Widths of spatial wavelets shown in Figure 3 plotted against $\sin \theta$, with θ being the maximum angle between diffractor and shot/receiver pairs. Each square is labeled with its corresponding aperture width. The drawn curve corresponds to equation (13).

by nonlinear effects for large apertures. Line lengths of 2500 m and more are unrealistically long compared to the depth of the diffractor at 500 m. This causes distortion of the wavelet.

Asymmetric aperture

In the previous sections, the diffractor was placed at the center of the midpoint range. It is of interest to investigate what happens for an asymmetric configuration, which may occur along the edge of a survey. Also, in single-fold 3-D data sets with limited extent (such as the cross-spread or a 3-D common-shot gather), the resolution may depend on the position of the output point with respect to the center of the data set.

Figure 6 describes a series of zero-offset experiments with constant midpoint range (500 m) and varying position of the diffractor. Figure 7 shows the resulting spatial wavelets for these experiments. The ideal spatial wavelet is also shown. The widest wavelet is obtained for the symmetric aperture (diffractor 1), whereas diffractors 2 and 3 lead to the better resolution represented by the next two wavelets. The spatial wavelet for diffractor 3 is virtually the same as for a symmetric experiment with line length 1000 m (cf. Figure 3). In other words, the maximum absolute wavenumber determines the resolution. With diffractor 3, we deal with a perfect one-sided operator which, at least in the actual diffraction point, is identical to the contribution that would have been obtained from the operator on the other side had the line extended also 500 m in that direction.

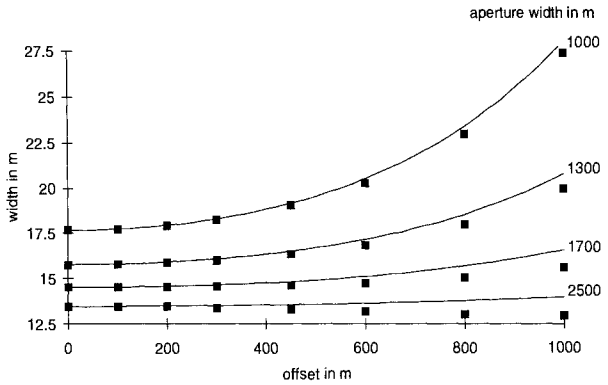

FIG. 5. Widths of spatial wavelets as a function of offset for line lengths 1000 (top), 1300, 1700, and 2500 m. The drawn curves correspond to equation (14).

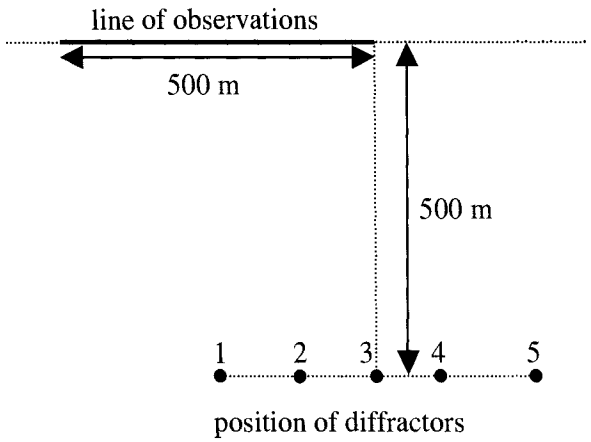

FIG. 6. Geometry for the asymmetry test.

For even larger aperture angles (diffractors 4 and 5), the central lobe continues to become smaller, at the expense of developing side lobes. For these diffractors, $k = 0$ does not occur in the wavenumber range, leading to incomplete spatial wavelets.

These results reveal a limitation of the resolution analysis using the spatial wavelet of a diffractor only as measured along the horizontal through the diffractor. Analysis of the full image would show its asymmetry for asymmetric input (Margrave, 1997). Mapping the configuration in the wavenumber domain would also show the asymmetry.

3-D spatial resolution

Up to this point, I only have discussed spatial resolution results for 2-D input. Next, I compare resolution of different minimal data sets (3-D single-fold data sets). For a fair comparison, the midpoint areas of the different configurations are equal to 1000×1000 m in all experiments. The diffractor is chosen in the center of the configuration at a depth of 500 m. Figure 8 shows the wavenumber spectra (computed from Beylkin's formula) for four different minimal data sets for two different input frequencies. The four boxes all have the same scale and, for ease of comparison, the positions of two corresponding points are indicated. The zero-offset wavenumber spectrum lies on a sphere with radius $|\mathbf{k}| = 2f/v$ [c.f. equation (4)]. For the wavenumber spectra of the other minimal data sets, $|\mathbf{k}| \leq 2f/v$ because of the NMO stretch effect. The 1000-m offset spectrum is strongly asymmetric; it is much wider in the cross-line direction than in the in-line direction. It is interesting to note that a single input frequency gives rise to a wide range of horizontal wavenumbers, including $k = 0$.

This should not be taken to mean that a single frequency is sufficient for optimal horizontal resolution (Vermeer, 1998a). It just means that the given midpoint range allows resolution in a wide range of directions (c.f. Figure 1). For a good resolution, it is still necessary to have a broad input spectrum, leading to a broad range of k-values in all those directions which have been illuminated by the range of input data. Yet, if we do have a broad spectrum, the maximum frequency or wavenumber may

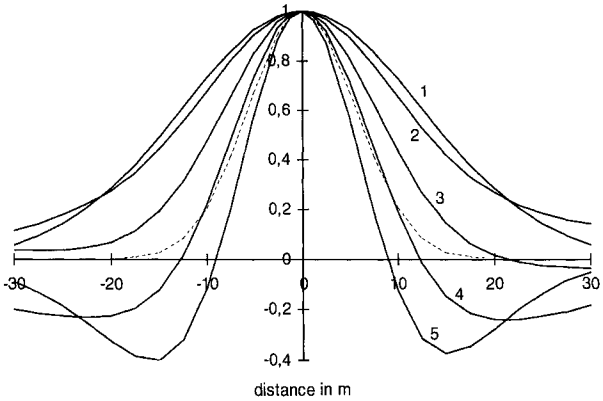

FIG. 7. Asymmetry test results. The spatial wavelets have been computed for the five diffractors shown in Figure 6, but have been plotted on top of each other for easier comparison. The width of the central loop becomes progressively smaller for diffractors 1–5. The ideal spatial wavelet is drawn as a dashed line for reference.

be taken as a main descriptor of resolution. In the case of the zero-offset section, the magnitude of **k** remains constant.

The maximum vertical wavenumber $k_{z,\max}$ of the zero-offset data, the cross-spread data, and the common-shot data is reached in the center of the plot: $k_{z,\max} = 2f/v$. For $f = f_{\max}$, this value gives an upper limit to the potential vertical resolution of any data set. Note, however, that the cross-spread and the 3-D shot reach this high value only for an output point right below the center of the data set. For output points away from the center, the maximum vertical wavenumber will be smaller, with correspondingly smaller potential resolution. The value at the center for the 1000-m offset data can be derived from equation (11) (and $R_z = c/2k_{z,\max}$) and equals $2f/(v\sqrt{2})$. The maximum value of k_z is somewhat larger (see Figure 8).

The projections on the horizontal wavenumber plane of the wavenumber spectra shown in Figure 8 are shown in Figure 9. The spectrum for 600-m offset is included as well. Figure 9 allows the prediction of the outcome of resolution tests for the five minimal data sets. The zero-offset section shows the broadest wavenumber range, followed by the 600-m offset data. Note the strong asymmetry of the spectrum for the 1000-m offset data. The 1000-m offset, the cross-spread, and the 3-D shot all have the same maximum wavenumber along the k_x-axis. This does not mean that these three data sets all have the same resolution in x. The maximum wavenumber as a function of k_y also plays a role. Maximum k_x does not vary as a function of k_y for the cross-spread, but it becomes smaller for the 1000-m offset gather and the 3-D shot; smallest for the 3-D shot.

Figure 10 shows the results of the computation of the spatial wavelets for the five minimal data sets discussed in Figure 9. For ease of comparison, the wavelets are not shown in an areal sense; only the wavelets for the x-coordinate are shown. For the 1000-m offset data the wavelet also is shown as computed for the cross-line direction. This wavelet nearly coincides with the wavelet for the in-line 600-m offset. This confirms once more that the resolution of offset data is better in the cross-line direction than in the in-line direction. The sequence of wavelet widths shown in Figure 10 is predicted by the wavenumber ranges shown in Figure 9.

The worst potential resolution is obtained for the 3-D shot. At first sight, this might be surprising because the diffraction traveltime surfaces as we know them are steeper for a common shot than for a zero-offset gather. However, this is the behavior of the diffraction traveltime curves on input, as a function of midpoint (x, y), whereas Beylkin's formula says that spatial resolution depends on the steepness of the traveltime curves as a function of the output coordinates.

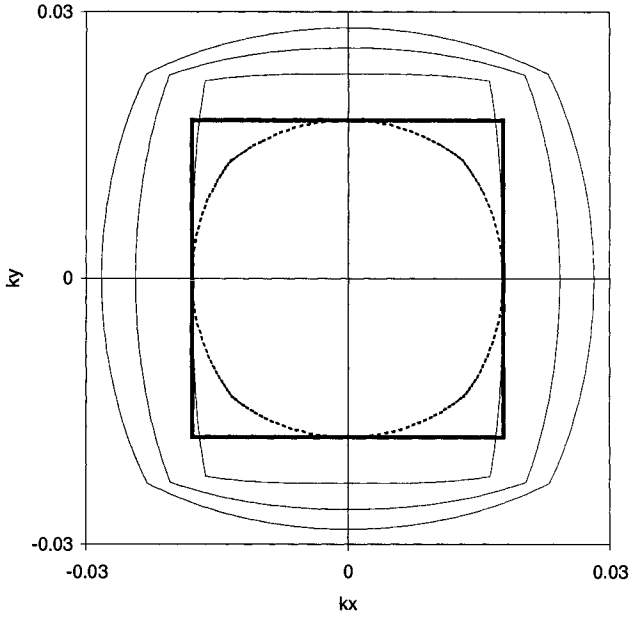

FIG. 9. Coverage in the horizontal wavenumber domain by five different minimal data sets with the same 1000 × 1000 midpoint area. The near circular shape in the center corresponds to the 3-D shot, the square to the cross-spread. The other three curves represent common-offsets 1000 m, 600 m, and 0 m. The largest wavenumbers are reached for the zero-offset section; hence, this section has the best spatial resolution.

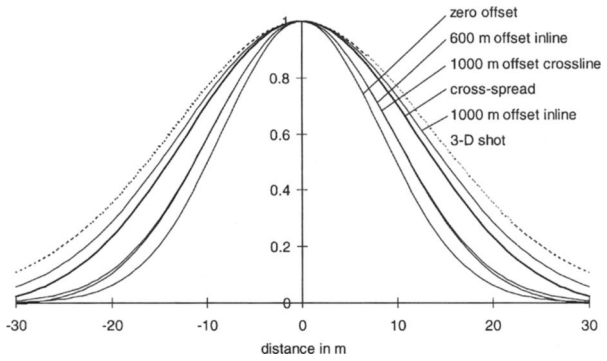

FIG. 10. Spatial wavelets for various minimal data sets. The zero-offset gather produces the narrowest wavelet, the 3-D common-shot gather the widest. Th curves for the 600-m in-line common offset and the 1000-m cross-line common offset nearly coincide. The relative widths of the wavelets confirm predictions based on Figure 9.

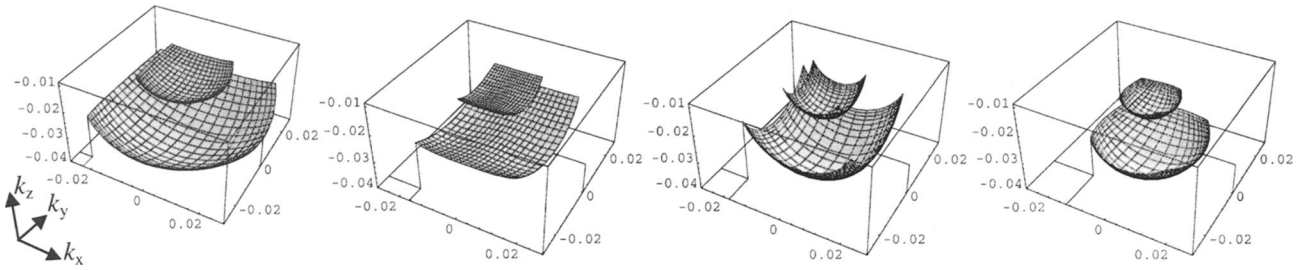

FIG. 8. Wavenumber spectra for four minimal data sets. All data sets have the same 1000 × 1000 m midpoint area with the diffractor in the center. The surfaces correspond to constant input frequencies. From left to right: zero-offset gather, 1000-m common-offset gather (with constant azimuth), cross-spread, and 3-D shot.

The results of Figure 10 confirm that the maximum wavenumber is not sufficient to predict the resolving power of a 3-D data set. Rather than the maximum wavenumber, it is the average maximum wavenumber taken for all k_y that turns out to determine the resolution in x. This can be understood by realizing that the result of the 3-D experiment can be considered as the average of the results of many 2-D experiments, each 2-D experiment consisting of data with constant y. The 2-D data with the largest y have a maximum k_x that is (usually) smaller than the data with $y=0$ and hence produce a wider spatial wavelet. Mathematically, the spatial wavelet of the whole 3-D data set is the normalized sum of the spatial wavelets of the contributing 2-D data sets.

The spatial wavelets shown thus far have all been normalized to the same maximum value to allow comparison of their relative widths. However, the discrimination against noise is also important. To get an idea about resolving power in the presence of noise, Figure 11 shows the "true amplitude" spatial wavelets for which no normalization has taken place. The small peak value and the relatively large tail value of the 3-D shot suggest that this configuration scores also worst as far as noise suppression is concerned. This aspect of geometry comparison is not further pursued in this paper.

Sampling and spatial resolution

The formulas for spatial resolution do not contain the sampling interval because these formulas have been derived for a continuous wavefield. If sampling takes place (which is inevitable, regardless whether we carry out modeling or real experiments), we sample the integrands of the migration formulas such as equation (12). If sampling is not rapid enough to keep up with the variations of the integrand (i.e., the integrand is aliased), unreliable results are produced, and resolution will suffer (see also the next section).

Despite the obvious importance of adequate sampling, there has been much discussion on the relation between sampling and resolution (Neidell, 1994, 1995; von Seggern, 1994; Ebrom et al., 1995a, b; etc.). Some of the results even seem to indicate that resolution is not significantly impaired by coarse sampling.

Coarse sampling does not influence the resolution of some model experiments because of the simplicity of the model. This can be illustrated with another simple experiment. In Figure 12, the spatial wavelets are shown for two 2-D geometries with the same line length of 1000 m, but different sampling intervals of 12.5 and 200 m. The wavelets are virtually identical except for the far end. The reason for this seemingly odd result is that the model only consists of the single diffractor. In output points close to the diffractor, the integrand in equation (12) varies only slowly as a function of ξ [the difference $\phi(\mathbf{x}, \xi) - \phi(0, \xi)$ is a slowly varying function of ξ; the other elements in the integrand vary slowly as well]. Hence, in this case, the large sampling interval of 200 m is dense enough to follow the variations of the integrand.

A similar reasoning can be applied to the results in von Seggern, (1994, his Figures 4 and 5). Those results seem to indicate even better resolution for the coarser sampling intervals, but that effect can be attributed to the fact that in that paper the effective spread length (the product of number of samples and sampling interval) of the experiments increases with increasing sampling interval.

Sampling and migration noise

In the previous section, it was shown that coarse sampling does not have much effect on resolution as measured with a single scatterer. However, migration of coarsely sampled input data produces so-called migration noise. In this section, the relation between sampling and migration noise is investigated.

To understand the effect of sampling on the migration result (and hence on spatial resolution), it is useful to describe the migration process as a two-step procedure (see Figure 13). First, the data are collected along the diffraction traveltime curves corresponding to the output point. This process converts all data contributing to that output point into a new data set, in which the diffraction produced by a diffractor in the output point is turned into a horizontal event (Figure 13b). A dipping event is turned into a bowl-shaped event with its apex at the position that has illuminated the output point, and with flanks that may be steeper than the dip in the input. The second step is to stack all this data into a single trace at the output point (Figure 13c).

The response of this second step can be described as a stack operator that depends on sampling (see Figure 14). For regular sampling, this operator has a passband around $k=1/d$, d being the spatial sampling interval. If the input data is coarsely sampled, it contains energy above $k_N=1/2d$. Then the migration operator moves some of this energy to higher

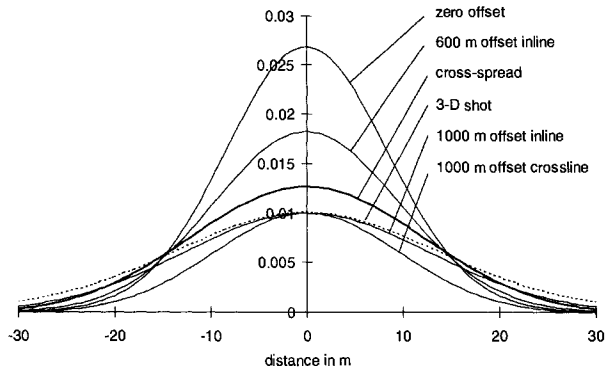

FIG. 11. "True-amplitude" spatial wavelets for same configurations as in Figure 10. The two solid curves with the same maximum at 0.01 correspond to the in-line and the cross-line resolutions of the 1000-m offset gather.

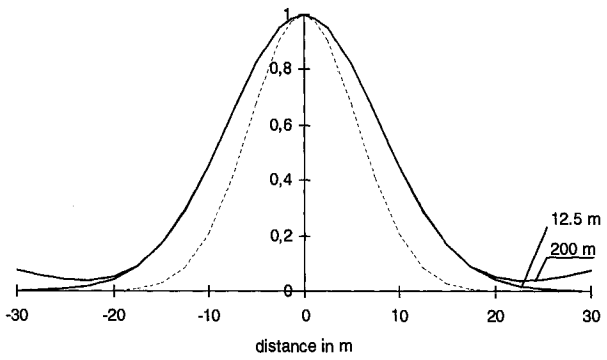

FIG. 12. Independence of spatial wavelet from spatial sampling. The two nearly coinciding outer wavelets correspond to 5 samples at 200 m and to 80 samples at 12.5 m. The narrow dotted curve is the ideal spatial wavelet.

wavenumbers and also to the passband at $k = 1/d$, allowing that energy to enter in the output. The stack operator of irregularly sampled data will not show a passband (d is not constant), and hence may better suppress energy above $k = 0$ than regularly sampled data. Therefore, random coarse sampling can be better than regular coarse sampling because it avoids the large peak in the response. On the other hand, if the input data is well sampled, there is no energy moving all the way to the passband at $k = 1/d$. Instead, with regular sampling, suppression of energy in the flanks of the operator benefits from the very low response around $k = 1/2d$, whereas the reward for doubling the sampling density in random sampling is only a reduction of 6 dB in the overall response. Hence, regular dense sampling gives much better suppression above $k = 0$ than random dense sampling.

This reasoning is put to the test with the experiments illustrated in Figure 15 for a horizontal event recorded by a 2-D zero-offset configuration. It shows vertical spatial wavelets with maximum amplitude normalized to 1. [Equation (12) does not include a phase-shift correction, therefore the reflection at 500 m is no longer zero phase.] The three leftmost wavelets have been produced by migrating input data sampled at 12.5, 25, and 33.3 m. The sampling interval of the other two wavelets was 33.3 m on average with random shifts of maximally 11.1 m on either side of the target sample points (the random shifts were generated using a uniform distribution). The figure shows that the event itself is (reasonably) well imaged in all cases, but that coarse sampling leads to migration noise above the event. The two rightmost wavelets illustrate the findings in Zhou and Schuster (1995) that quasi-random sampling may reduce migration noise.

In practice (assuming that quasi-random sampling is a practical proposition, which I doubt), apparent velocities in the wavefield made up of reflections and diffractions may be larger than those of coherent ground roll events. In that case, the desired signal may be properly sampled by using a dense sampling, whereas the coherent noise is still undersampled. Under these conditions, the coherent noise would be better suppressed by quasi-random dense sampling, whereas the desired signal would be best served with regular dense sampling. This dilemma is not solved here.

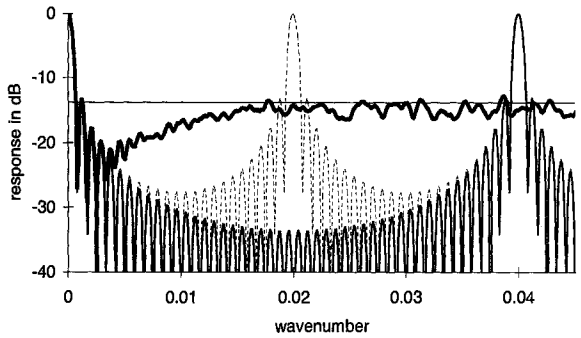

FIG. 14. Stack responses of regular dense sampling (sampling interval 25 m, first passband at $k = 0.04$, thin line), regular coarse sampling (sampling interval 50 m, first passband at $k = 0.02$, dotted line), and random coarse sampling (sampling interval 50 m on average, average of 50 realizations, no passbands, heavy line). Horizontal line indicates level of random noise suppression. Note that random sampling removes strong peak(s), but cannot match rejection of regular dense sampling in central part of wavenumber axis.

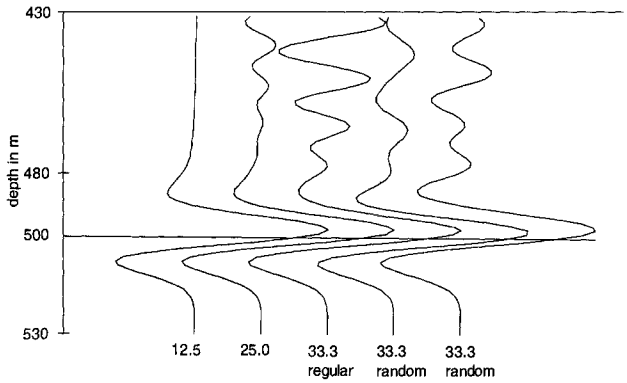

FIG. 15. Effect of sampling interval on migration noise for horizontal reflection. Input spatial sampling intervals are (from left to right): 12.5 m, 25 m, 33.3 m, and two random samplings with 33.3 m interval on average. The two rightmost curves (random sampling of input) show somewhat less migration noise than the central curve for which the input data were regularly sampled at 33.3 m. Note that regular sampling with a smaller sampling interval of 25 m (second curve from the left) produces less migration noise than the random input.

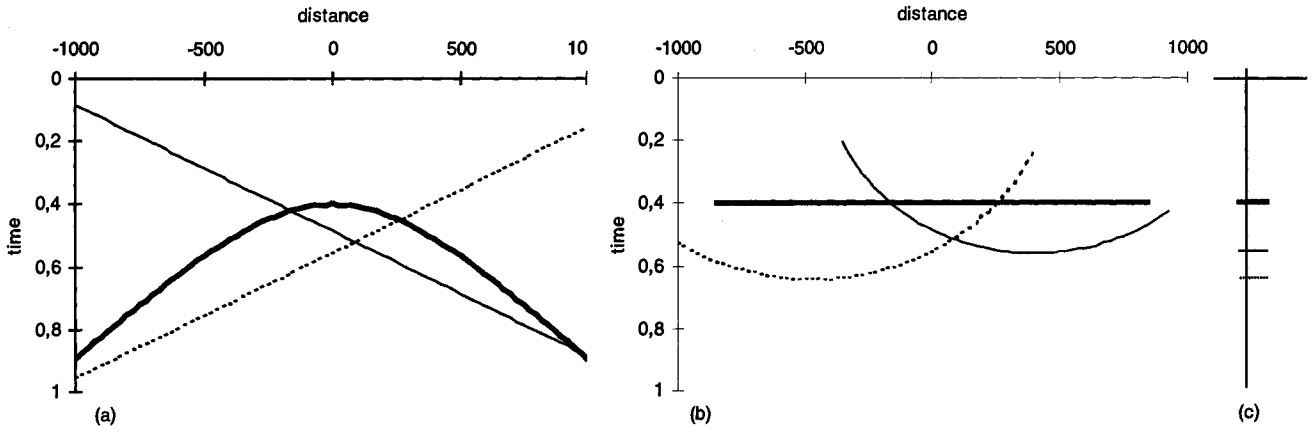

FIG. 13. Migration as a two-step process illustrated with 2-D zero-offset section. (a) Input showing diffraction (heavy curve) and two dipping events (thin curves). (b) In the first step, the input data are realigned according to the diffraction traveltimes in the output point. Shown is the realignment for the output point at $x = 0$, which is the position of the diffractor. (c) In the second step, the realigned data are summed (stacked) to form one output trace. The response of the second step depends on the sampling of the input data and is illustrated in Figure 14.

The suppression of random noise, of course, is independent of the sampling regime; it would only depend on the number of samples contributing to each output sample.

Bin fractionation

Bin fractionation and flexi-bin are acquisition techniques for orthogonal geometries which achieve finer midpoint spacing than the natural bin size following from the shot and receiver station intervals (Cordsen, 1993; GRI, 1994; Flentge, 1997). Figure 16 illustrates the bin-fractionation technique. (In the flexi-bin technique, a finer distribution of midpoints is achieved by choosing line intervals which are a noninteger multiple of the station intervals.) The question is: will the finer midpoint spacing lead to better resolution?

With the bin-fractionation technique, the same cross-spreads are acquired as in conventional acquisition with shot and receiver locations not staggered. The only difference are the sample positions. From the discussion in this paper, it should be clear that potential resolution (being independent of sampling) cannot be improved with the bin-fractionation technique. If an improvement in resolution is to be achieved, it should be the result of less sensitivity to coarse sampling, i.e., bin fractionation should produce less migration noise for the same coarse sampling intervals.

The interleaving of cross-spreads using the bin-fractionation technique may be compared with the interleaving of zero-offset data sets. Two or more coarsely sampled but interleaved zero-offset data sets form a new zero-offset data set with finer sampling. The migration result of the combined data set will show less migration noise than each of the original zero-offset data sets because their migration noises are largely in antiphase. However, overlapping and interleaved cross-spreads do not form a new and better sampled single cross-spread. Therefore, the migration noises of the cross-spreads will in general not be in antiphase with each other, and just reduce each other according to rules of fold. Even though the midpoint sampling has improved, the sampling of the subsurface (illumination) has not in general improved.

This reasoning is tested in Figure 17. It shows that coarsely sampled interleaved zero-offset sections lead to a significant reduction in migration noise when merged (leftmost curves).

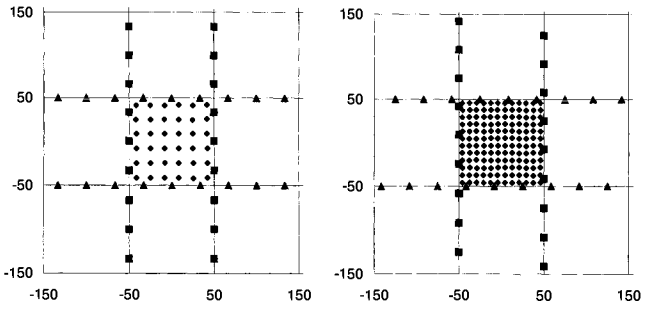

FIG. 16. Sampling schemes in orthogonal geometry. Left: conventional, right: bin fractionation. Squares and triangles represent shotpoint and receiver locations, respectively. Diamonds represent the midpoint positions. The distance between midpoints with bin fractionation is one quarter of the distance between the stations (in this example).

Also, a densely sampled cross-spread does not produce much migration noise (rightmost curve). On the other hand, regular coarse sampling of cross-spreads and staggered coarse sampling of cross-spreads produce similar amounts of migration noise, also after merging (central curves).

Fold and spatial resolution

The analysis of spatial resolution as given in Beylkin et al. (1985) deals with single-fold 3-D data. As discussed above, it assumes implicitly that the temporal and two spatial coordinates have been sampled properly. If N-fold data are used, ideally the data can be split into N such well-sampled single-fold subsets (Vermeer, 1998c). For each subset, the potential resolution can be analyzed. The resolution of the stack of the N migration results will be some average of the resolutions of the contributing subsets (in the absence of any noise that does not satisfy the velocity model; otherwise, such noises would influence the resolvability of close events). As the best possible resolution for a given midpoint range can be obtained with a 3-D single-fold zero-offset gather, the resolution of the stack will be less good than the resolution of that zero-offset gather. More on this subject can be found in Levin (1998), where minimal data sets are called "nonredundant data subsets."

In case each contributing subset of an N-fold data set is undersampled, giving rise to migration noise for each subset, then the stack of the N single-fold migration results would reduce the noise. Now the achievable resolution (in any direction) of the stack of the N migration results should be better than the achievable resolutions of the contributing subsets. Yet, even with very large N, resolution cannot become better than the limit imposed by the maximum frequency in the input data. In an interesting physical modeling experiment, Markley et al. (1996) show that fold improves resolution of coarsely sampled data, but that the result cannot match the resolution of well-sampled single-fold data.

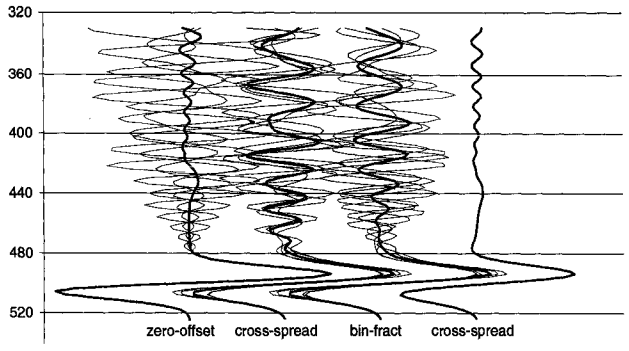

FIG. 17. Migration noise for different acquisition strategies, measured on a dipping event. The thin curves represent coarsely sampled configurations with sampling interval of 33 m. From left to right: four zero-offset data sets, four regularly sampled cross-spreads, and four cross-spreads sampled as indicated in Figure 16 on the right. The heavy curves are the averaged results of each group of four coarsely sampled data sets. The rightmost curve is the result for a single cross-spread with 16.5-m shot and receiver station spacings. Note that bin fractionation does not lead to a significant reduction of migration noise.

DISCUSSION

All observations and conclusions in this paper have been derived for a simple constant-velocity model. As such they provide valuable insight into various factors affecting spatial resolution, but what about more complex models? In my opinion, the results of this paper can be used as a first-order approximation to more complex situations. In case of doubt about the applicability to more complex models, it is recommended to apply Beylkin's formula to those models. The main requirement is that the diffraction traveltimes can be computed for the given velocity model and measurement configuration (acquisition geometry and source wavelet). To avoid that fold will confuse the issue, it is important to investigate resolution for separate minimal data sets.

The theoretically best possible resolution (the potential resolution) cannot be improved by better sampling because it already assumes perfect sampling. This truism applies to any measurement model, not just to the simple model investigated in this paper. However, it tends to be overlooked in discussions on the relation between sampling and resolution. Neidell (1997) denies the truism: "According to the Huygens' approach, achievable resolution can be increased almost without limit if we increase the redundancy of the wavefield sampling." Indeed, redundancy may increase achievable resolution by reduction of noise and a more accurate evaluation of the migration integrals, but the limits set by Beylkin's formula (maximum frequency of the source wavelet and steepest time dips in the diffraction traveltime surfaces) cannot be tresspassed.

On the other hand, Beylkin's formula only sets limits on the range of wavenumbers. How this translates into minimum resolvable distance depends on the proportionality factor c. If amplitude information can be used [see remark following equation (7b)] or if additional information is available [e.g., well information (Levin, 1998), or smoothness of an interface], c may be considerably smaller than the value 0.71 following from the Rayleigh criterion. This elusiveness of c might be the reason of much confusion in resolution discussions.

The nature of the surface seismic acquisition technique causes a difference between vertical and horizontal resolution. It also causes a difference between the wavelets. In our case, the Ricker wavelet remains a Ricker wavelet in the vertical direction, but it turns into a Gaussian in the horizontal directions. Different wavelets lead to different resolution measurements (Kallweit and Wood, 1982). This difference leads to a complication when trying to compare horizontal and vertical resolution on basis of measurements of the width of the main lobe of the wavelet. I have dodged this issue by comparing only wavelets in the horizontal direction for various situations; I only looked at the vertical direction to investigate migration noise. Beylkin's formula is available to compute the range of wavenumbers in (k_x, k_y, k_z)-space allowing a comparison of those ranges in x, y, and z.

The results for the bin-fractionation technique show that the sampling of the minimal data sets of the geometry (cross-spreads in this case) determines the achievable resolution, and not the sampling density of the midpoints. On the other hand, increasing the midpoint sampling density of the zero-offset gathers did help, because now the midpoint sampling also determines the sampling of the minimal data set. This raises an interesting question about some intermediate situations. In marine streamer acquisition, the fold-of-coverage is smaller than the number of different offsets (for single streamer and source interval equal to or larger than the group interval). This means that each offset is undersampled, and full single-fold coverage can only be achieved by combining two or more neighboring offsets. Would the migration noise produced by the merged common-offset gathers be similarly reduced as for the zero-offset gather in Figure 16, or would it be more like the results for the two sets of cross-spreads shown in that figure? I suspect that the merged gather is close enough to a minimal data set to benefit from the denser midpoint sampling, but this needs confirmation by further research.

Multisource multistreamer configurations cannot produce 3-D single-fold subsets which are well sampled (Vermeer, 1994, 1997). The shot/receiver azimuths in the common-offset gathers of these surveys vary in a discontinuous way. As a consequence, the diffraction traveltime curves in these gathers will show irregularities, leading to some loss of achievable resolution. Differential feathering between streamers may aggravate the problem. To what extent the spatial irregularities of these and other geometries influence achievable resolution is a matter of further research.

CONCLUSIONS

In this paper, I have linked the description of spatial resolution given in Beylkin et al. (1985) to the more heuristic approach to spatial resolution as given in, for example, Ebrom et al. (1995a). The simple resolution formulas that apply to 2-D data provide a lower limit to the minimum resolvable distance that can be achieved with 3-D data.

Potential resolution (theoretically best possible resolution for a given geometry and a correct velocity model) is determined by the spatial gradients of the diffraction traveltime curves and the source wavelet. Beylkin's formula links these gradients to spatial wavenumbers.

Surface seismic data produce spatial resolutions that are different in the horizontal and vertical directions. In this paper, only constant-velocity models have been investigated. For those models, horizontal resolution is determined mainly by aperture of the seismic experiment and by the maximum frequency in the source wavelet. The horizontal resolution also depends on the seismic experiment configuration: for the same range of midpoints, common-offset data have lower potential resolution than zero-offset data, and in the in-line direction, resolution of common-offset data is lower than in the cross-line direction. Cross-spreads have better potential resolution than 3-D common-shot gathers, but have in general worse resolution than common-offset gathers. This puts some ranking on the corresponding acquisition geometries. The vertical resolution does not depend on aperture, but does depend on maximum frequency and offset.

Potential resolution assumes perfect sampling. Sampling influences the correctness of the migration process to a large extent because sampling is a way of approximating the migration integration formulas as derived for continuous shot and receiver variables. Invalid migration results are obtained as soon as the integrand in those formulas varies more rapidly than sampling can follow, i.e., as soon as the data are aliased along the integration paths.

Migration noise (caused by coarse sampling) can also be reduced by using quasi-random sampling instead of regular sampling. However, as dense regular sampling would minimize migration noise, quasi-random coarse sampling cannot match the quality obtainable with regular dense sampling.

Staggered sampling of the acquisition lines (the bin-fractionation technique) produces a denser sampling of midpoints, but it does not compensate for coarse sampling.

Noise in the data will reduce the achievable resolution. Therefore, increasing fold will virtually always improve achievable resolution, even though it would in general not improve potential resolution. This applies to noise in the form of ambient noise, ground roll, and multiples, as well as to migration noise caused by coarse sampling.

All results and conclusions are based on investigations using a simple constant-velocity model. As such, it provides some valuable insights, which might also apply to more complex models.

ACKNOWLEDGMENTS

I thank Kees Hornman for drawing my attention to this subject and for continuing discussions. During various stages of writing this paper, (former) Shell colleagues Matthias Brühl, Jaap Mondt, Arie Verdel, Ep de Jonge, and Stéphane Gesbert were active discussion partners. Discussions with Joe Higginbotham, Dan Ebrom, Helmut Jakubowicz, and Bill Goodway helped shape the first version of this paper prepared for the 3-D Sampling Workshop at the 1996 SEG Annual Meeting in Denver. The SEG reviewers were generous with critical remarks, for which I am most grateful. I also like to thank Jaap Vermeer, who converted my slow Mathematica program to a speedy program in C. I am grateful to Shell International Exploration and Production B.V. for support received in preparing this paper.

REFERENCES

Bednar, J. B., 1996, Coarse is coarse of course unless. . . : The Leading Edge, **15**, 763–764.

Berkhout, A. J., 1984, Seismic resolution—A quantitative analysis of resolving power of acoustical echo techniques: Geophysical Press.

Beylkin, G., 1985, Imaging of discontinuities in the inverse scattering problem by inversion of a causal generalized Radon transform: J. Math. Phys. **26**, 99–108.

Beylkin, G., Oristaglio, M., and Miller, D., 1985, Spatial resolution of migration algorithms, *in* Berkhout, A. J., Ridder, J., and van der Waals, L. F., Eds., Proc. 14th Internat. Symp. on Acoust. Imag., 155–167.

Bleistein, N., 1987, On the imaging of reflectors in the earth: Geophysics, **52**, 931–942.

Cohen, J. K., Hagin, F. G., and Bleistein, N., 1986, Three-dimensional Born inversion with an arbitrary reference: Geophysics, **51**, 1552–1558.

Cordsen, A., 1993, Flexi-bin 3-D seismic acquisition method: Can. Soc. Expl. Geophys. Ann. Mtg. Abstracts, 19.

Devaney, A. J., 1984, Geophysical diffraction tomography: IEEE Trans. Geosci. Remote Sensing, **GE-22**, 3–13.

Ebrom, D., Li, X., McDonald, J., and Lu, L., 1995a, Bin spacing in land 3-D seismic surveys and horizontal resolution in timeslices: The Leading Edge, **14**, No. 1, 37–40.

Ebrom, D. A., Sekharan, K. K., McDonald, J. A., and Markley, S. A., 1995b, Interpretability and resolution in post-migration time-slices: 65th Ann. Internat. Mtg., Soc. Expl. Geophys., Expanded Abstracts, 995–998.

Flentge, D. M., 1997, Method of performing high resolution crossed-array seismic surveys: U.S. Patent 5 598 378.

Gibson, R. L., Tzimeas, C., and Lavely, E., 1998, Seismic survey design for optimal imaging and resolution of elastic properties: 1998 EAGE/SEG Summer Research Workshop, Depth Imaging of Reservoir Attributes, Extended Abstracts, paper X002.

Goulty, N. R., 1997, Crosswell seismic reflection imaging of field data sets: the need for migration: First Break, **15**, 325–330.

GRI (Gas Research Institute), 1994, Staggered-line 3-D seismic recording: A technical summary of research conducted for Gas Research Institute, the U.S. Department of Energy, and the State of Texas by the Bureau of Economic Geology, The University of Texas at Austin.

Kallweit, R. S., and Wood, L. C., 1982, The limits of resolution of zero-phase wavelets: Geophysics, **47**, 1035–1046.

Knapp, R. W., 1990, Vertical resolution of thick beds, thin beds, and thin-bed cyclothems: Geophysics, **55**, 1183–1190.

Lavely, E., Gibson, R. L., and Tzimeas, C., 1997, 3-D seismic survey design for optimal resolution: Presented at the 67th Ann. Internat. Mtg., Soc. Expl. Geophys., paper ACQ2.2.

Levin, S. A., 1998, Resolution in seismic imaging: Is it all a matter of perspective?: Geophysics, **63**, 743–749.

Markley, S. A., Ebrom, D. A., Sekharan, K. K., and McDonald, J. A., 1996, The effect of fold on horizontal resolution in a physical model experiment: 66th Ann. Internat. Mtg., Soc. Expl. Geophys., Expanded Abstracts, ACQ2.2.

Margrave, G. F., 1997, Seismic acquisition parameter considerations for a linear velocity medium: Presented at the 67th Ann. Internat. Mtg., Soc. Expl. Geophys., paper ACQ2.6.

Neidell, N. S., 1994, Sampling 3-D seismic surveys: A conjecture favoring coarser but higher-fold sampling: The Leading Edge, **13**, 764–768.

——— 1995, Round Table, Is "coarse" the right course? *Reply*: The Leading Edge, **14**, 989–990.

——— 1997, Perceptions in seismic imaging, Part 4: Resolution considerations in imaging propagation media as distinct from wavefields: The Leading Edge, **16**, 1412–1415.

Padhi, T., and Holley, T. K., 1997, Wide azimuths—why not?: The Leading Edge, **16**, 175–177.

Safar, M. H., 1985, On the lateral resolution achieved by Kirchhoff migration: Geophysics, **50**, 1091–1099.

Sun, Y., Schuster, G. T., and Sikorski, K., 1997, A quasi-Monte Carlo approach to 3-D migration: Theory: Geophysics, **62**, 918–928.

Tygel, M., Schleicher, J., and Hubral, P., 1994, Pulse distortion in depth migration: Geophysics, **59**, 1561–1569.

Vermeer, G. J. O., 1994, 3-D symmetric sampling: 64th Ann. Internat. Mtg., Soc. Expl. Geophys., Expanded Abstracts, 906–909.

——— 1995, Round Table, Is "coarse" the right course?: The Leading Edge, **14**, 989–990.

——— 1997, Streamers versus stationary receivers: Proc. Offshore Tech. Conf., paper OTC8314, 331–346.

——— 1998a, Factors affecting spatial resolution: The Leading Edge, **17**, 1025–1030, 1161.

——— 1998b, Discussion on: "A quasi-Monte Carlo approach to 3-D migration: Theory," Sun, Y., Schuster, G. T., and Sikorski, K., authors: Geophysics, **63**, 1475.

——— 1998c, 3-D symmetric sampling: Geophysics, **63**, 1629–1647.

von Seggern, D., 1991, Spatial resolution of acoustic imaging with the Born approximation: Geophysics, **56**, 1185–1202.

——— 1994, Depth-imaging resolution of 3-D seismic recording patterns: Geophysics, **59**, 564–576.

Wu, R-S., and Toksöz, M. N., 1987, Diffraction tomography and multisource holography applied to seismic imaging: Geophysics, **52**, 11–25.

Zhou, C., and Schuster, G. T., 1995, Quasi-random migration of 3-D field data: 65th Ann. Internat. Mtg., Soc. Expl. Geophys., Expanded Abstracts, 1145–1148.